COMMUNICATIONS IN NUMERICAL METHODS IN ENGINEERING
Commun. Numer. Meth. Engng 2005; **21**:433–442
Published online 15 March 2005 in Wiley InterScience (www.interscience.wiley.com). DOI: 10.1002/cnm.758

Structural optimization by simultaneous equilibration of spatial and material forces

Harm Askes[1], Swantje Bargmann[2], Ellen Kuhl[2] and Paul Steinmann[2,*,†]

[1]*Department of Civil and Structural Engineering, University of Sheffield, Sheffield S1 3JD, U.K.*
[2]*Faculty of Mechanical Engineering, University of Kaiserslautern, 67653 Kaiserslautern, Germany*

SUMMARY

In this contribution, a dual equilibrium methodology is applied to the shape optimization of trusses. The spatial co-ordinates as well as the material (i.e. initial) co-ordinates of the joints are taken as unknowns in the potential energy of the structure whereby the connectivity is fixed. The conjugated variables, i.e. spatial forces and material forces, are equilibrated. Whereas equilibration of the spatial forces is equivalent to finding the optimal joint displacements, equilibration of the material forces yields the optimal initial joint positions. The two sets of equilibrium equations are derived and solved in a completely coupled manner. With a proper linearization and a Newton–Raphson scheme, shape optimization of the truss can be achieved within a few iterations. This is demonstrated by two numerical examples. Copyright © 2005 John Wiley & Sons, Ltd.

KEY WORDS: truss; optimization; material forces; dual equilibrium; arbitrary Lagrangian–Eulerian

1. INTRODUCTION

Optimization of trusses can be performed in many ways, depending on the objective function. Normally, the design parameters are taken as the joint positions and the cross sectional area of the truss members. Typical objective functions are total weight of the structure or displacements at certain critical joints [1]. Here, a truss optimization algorithm is proposed that is firmly rooted in mechanics and developed in terms of a variational principle of the Dirichlet type. Thereby, we closely follow an approach recently suggested in References [2, 3], which will be extended to the geometrically non-linear regime. To this end, the potential energy of the structure is taken as an explicit function of the final (deformed) as well as the initial (undeformed) positions of the joints. Next, the potential energy is optimized with respect to these two sets of variables, which is equivalent to the equilibration of the conjugated force-type quantities. The forces as they are commonly known are the forces that are conjugated

*Correspondence to: Paul Steinmann, Faculty of Mechanical Engineering, University of Kaiserslautern, D-67653 Kaiserslautern, Germany.
†E-mail: ps@rhrk.uni-kl.de

Copyright © 2005 John Wiley & Sons, Ltd.
Received 3 August 2004
Accepted 18 January 2005

to the final positions of the joints, or in other words the co-ordinates of the joints in the *spatial configuration*—hence these forces are denoted here as *spatial forces*. Conversely, the *material forces* are conjugated to the initial positions of the joints, or the co-ordinates in the *material configuration* [4, 5].

The duality between the spatial force equilibrium and the material force equilibrium has been discussed and elaborated extensively in References [6–9]. A material force residual indicates an inhomogeneity, and typical occurrences of material forces include the Peach–Koehler force on dislocations and the J-integral in fracture mechanics. More recently, it was recognized that material forces can also occur as a result of discretization of the continuum equations, e.g. in finite element simulations [2, 10]. Indeed, additional energy can be released by moving the nodes of the finite element mesh opposite to the corresponding material force residual, by which mesh optimization algorithms can be devised. The mesh optimization can be performed *after* the equilibration of the spatial forces [2, 10, 11] or the two sets of equilibrium equations can be solved *simultaneously* [12, 13]. The latter approach has the advantage that far less iterations are needed to arrive at the optimal mesh configuration [13].

In this contribution, the dual equilibrium approach is applied to the optimization of trusses, see also References [2, 3]. The same framework as developed for mesh optimization in References [12, 13] is used, the difference being that now the geometric description of the structure changes within the optimization process. In an earlier work, the material joint positions were determined after solving the equilibrium of spatial forces [3] for a geometrically and materially linear setting; here, the two sets of equilibrium equations are developed and solved simultaneously in the spirit of References [12, 13]. A non-linear Neo-Hookean elastic material model is assumed. After briefly restating the governing equations, two examples are treated: one benchmark example for which the analytical solution of the infinitesimal strain case is known, and a more elaborate example.

It is emphasized that in the context of structural optimization, the present application deals solely with the shape optimization of trusses (i.e. joint positions), not the size optimization (i.e. cross sectional areas of the members) nor the connectivity optimization (i.e. the topology). Furthermore, it is assumed that the external forces are significantly larger than the dead weight of the truss, so that minimization of weight can be ignored in favour of the minimization of potential energy.

2. GOVERNING EQUATIONS

As mentioned above, both the spatial configuration $\mathscr{B}_t$ and the material configuration $\mathscr{B}_0$ are unknown. Therefore, a third, independent domain $\mathscr{B}_\square$ must be introduced as a reference configuration, cf. Figure 1. The underlying kinematic description is known as the arbitrary Lagrangian–Eulerian (ALE) technique, see Reference [12]. The fundamental idea of the particular ALE approach considered herein is the reformulation of the spatial and material deformation maps $\boldsymbol{\varphi}$ and $\boldsymbol{\Phi}$ as a decomposition of the two referential mappings $\bar{\boldsymbol{\varphi}}$ and $\tilde{\boldsymbol{\Phi}}$ as $\boldsymbol{\varphi} = \bar{\boldsymbol{\varphi}} \circ \tilde{\boldsymbol{\Phi}}^{-1}$ and $\boldsymbol{\Phi} = \tilde{\boldsymbol{\Phi}} \circ \bar{\boldsymbol{\varphi}}^{-1}$.

The corresponding variational setting for hyperelastic conservative systems is then defined in terms of the ALE Dirichlet principle characterized through the vanishing total variation of the overall truss energy $\delta\mathscr{I}$ at fixed referential co-ordinates ξ

$$\delta\mathscr{I} = \delta_{\mathbf{x}}\mathscr{I} + \delta_{\mathbf{X}}\mathscr{I} \doteq 0 \tag{1}$$

Copyright © 2005 John Wiley & Sons, Ltd.

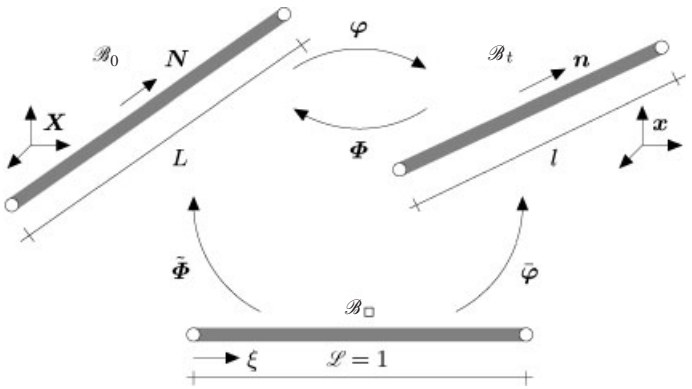

Figure 1. ALE kinematics of truss element.

Now, the essential idea of the proposed method is to replace this total variation by a variation with respect to the spatial co-ordinates **x** at fixed material co-ordinates **X** plus a variation with respect to the material co-ordinates **X** at fixed spatial co-ordinates **x**. For the truss structures considered herein, these spatial and material variations take the following discrete formats:

$$\delta_{\boldsymbol{x}}\mathscr{I}=\sum_{I=1}^{n_{\text{tn}}}\delta\bar{\boldsymbol{\varphi}}_I\cdot\mathbf{R}^I_{\bar{\varphi}},\quad \delta_{\mathbf{X}}\mathscr{I}=\sum_{J=1}^{n_{\text{tn}}}\delta\tilde{\boldsymbol{\Phi}}_J\cdot\mathbf{R}^J_{\tilde{\Phi}} \tag{2}$$

based on the elementwise discretization of the spatial and material joint positions $\bar{\boldsymbol{\varphi}}$ and $\tilde{\boldsymbol{\Phi}}$ and their variations $\delta\bar{\boldsymbol{\varphi}}$ and $\delta\tilde{\boldsymbol{\Phi}}$

$$\delta\bar{\boldsymbol{\varphi}}^h|_{\mathscr{B}^e_\square}=\sum_{i=1}^{n_{\text{en}}}N^i_{\bar{\varphi}}\delta\bar{\boldsymbol{\varphi}}_i,\quad \bar{\boldsymbol{\varphi}}^h|_{\mathscr{B}^e_\square}=\sum_{k=1}^{n_{\text{en}}}N^k_{\bar{\varphi}}\bar{\boldsymbol{\varphi}}_k,\quad \delta\tilde{\boldsymbol{\Phi}}^h|_{\mathscr{B}^e_\square}=\sum_{j=1}^{n_{\text{en}}}N^j_{\tilde{\Phi}}\delta\tilde{\boldsymbol{\Phi}}_j,\quad \tilde{\boldsymbol{\Phi}}^h|_{\mathscr{B}^e_\square}=\sum_{l=1}^{n_{\text{en}}}N^l_{\tilde{\Phi}}\tilde{\boldsymbol{\Phi}}_l \tag{3}$$

in terms of the linear shape functions $N^i_{\bar{\varphi}}$ and $N^j_{\tilde{\Phi}}$ with $N_{\bar{\varphi},\tilde{\Phi}}=[1-\xi;+\xi]$. For arbitrary variations $\delta\bar{\boldsymbol{\varphi}}_I$ and $\delta\tilde{\boldsymbol{\Phi}}_J$, Equations (2) are equivalent to the vanishing discrete spatial and material residuals $\mathbf{R}^I_{\bar{\varphi}}$ and $\mathbf{R}^J_{\tilde{\Phi}}$, i.e. the difference of the corresponding internal and external forces

$$\mathbf{R}^I_{\bar{\varphi}}(\bar{\boldsymbol{\varphi}}^h,\tilde{\boldsymbol{\Phi}}^h)=\mathop{\mathbf{A}}_{t=1}^{n_{\text{tr}}}\nabla_\xi N^i_{\bar{\varphi}}\Pi A\mathbf{n}-\mathbf{F}^{\text{ext}\,I}_{\bar{\varphi}}\doteq\mathbf{0},\quad \mathbf{R}^J_{\tilde{\Phi}}(\bar{\boldsymbol{\varphi}}^h,\tilde{\boldsymbol{\Phi}}^h)=\mathop{\mathbf{A}}_{t=1}^{n_{\text{tr}}}\nabla_\xi N^j_{\tilde{\Phi}}\pi A\mathbf{N}-\mathbf{F}^{\text{ext}\,J}_{\tilde{\Phi}}\doteq\mathbf{0} \tag{4}$$

Thereby, $\mathbf{A}_{t=1}^{n_{\text{tr}}}$ symbolizes the assembly over all $t=1,\ldots,n_{\text{tr}}$ truss member contributions at the $i,j=1,\ldots,n_{\text{en}}$ member joints to the global spatial and material internal forces at all $I,J=1,\ldots,n_{\text{tn}}$ global joints, whereas $\mathbf{F}^{\text{ext}\,I}_{\bar{\varphi}}$ and $\mathbf{F}^{\text{ext}\,J}_{\tilde{\Phi}}$ denote the corresponding external forces on the $I,J=1,\ldots,n_{\text{tn}}$ global joints. The referential gradient of the shape functions is given as $\nabla_\xi N_{\bar{\varphi},\tilde{\Phi}}=[-1;+1]$. For the hyperelastic case considered herein, the spatial and material stresses $\Pi=\mathrm{D}_F W_0$ and $\pi=\mathrm{d}_f W_t$ can be introduced in terms of the free energy densities of the

Copyright © 2005 John Wiley & Sons, Ltd.

spatial and the material motion problem, e.g. of Neo-Hookean type, as $W_0 = \frac{1}{4} E_0[F^2 - 1 - 2\ln(F)]$ and $W_t = \frac{1}{4} E_0[1/f - f - 2f\ln(1/f)]$ as $W_t = W_0/F$

$$\Pi = \frac{1}{2} E_0 \left[F - \frac{1}{F} \right], \quad \pi = \frac{1}{4} E_0 \left[-\frac{1}{f^2} + 1 - 2\ln\left(\frac{1}{f}\right) \right] \tag{5}$$

The spatial and material stretches $F = l/L$ and $f = L/l$ are defined in terms of the spatial and material member lengths l and L. Moreover, upon discretization, the corresponding element normals $\mathbf{n}$ and $\mathbf{N}$ take the following discrete formats:

$$\begin{aligned} l &= \left\| \sum_{i=1}^{n_{\text{en}}} \bar{\boldsymbol{\varphi}}_i \nabla_\xi N^i_{\bar{\varphi}} \right\| = \bar{F}, \quad L = \left\| \sum_{j=1}^{n_{\text{en}}} \tilde{\boldsymbol{\Phi}}_j \nabla_\xi N^j_{\tilde{\Phi}} \right\| = \tilde{f} \\ \mathbf{n} &= \frac{\sum_{i=1}^{n_{\text{en}}} \bar{\boldsymbol{\varphi}}_i \nabla_\xi N^i_{\bar{\varphi}}}{\| \sum_{i=1}^{n_{\text{en}}} \bar{\boldsymbol{\varphi}}_i \nabla_\xi N^i_{\bar{\varphi}} \|}, \qquad \mathbf{N} = \frac{\sum_{j=1}^{n_{\text{en}}} \tilde{\boldsymbol{\Phi}}_j \nabla_\xi N^j_{\tilde{\Phi}}}{\| \sum_{j=1}^{n_{\text{en}}} \tilde{\boldsymbol{\Phi}}_j \nabla_\xi N^j_{\tilde{\Phi}} \|} \end{aligned} \tag{6}$$

For the solution of the non-linear coupled system of Equations (4) we suggest an incremental iterative Newton–Raphson solution technique based on the consistent linearization of the residuals

$$\begin{aligned} \mathbf{R}^{I\,k+1}_{\bar{\varphi}} &= \mathbf{R}^{I\,k}_{\bar{\varphi}} + \sum_{K=1}^{n_{\text{tn}}} \mathbf{K}^{IK}_{\bar{\varphi}\bar{\varphi}} \, \mathrm{d}\bar{\boldsymbol{\varphi}}_K + \sum_{L=1}^{n_{\text{tn}}} \mathbf{K}^{IL}_{\bar{\varphi}\tilde{\Phi}} \, \mathrm{d}\tilde{\boldsymbol{\Phi}}_L \doteq \mathbf{0} \\ \mathbf{R}^{J\,k+1}_{\tilde{\Phi}} &= \mathbf{R}^{J\,k}_{\tilde{\Phi}} + \sum_{K=1}^{n_{\text{tn}}} \mathbf{K}^{JK}_{\tilde{\Phi}\bar{\varphi}} \, \mathrm{d}\bar{\boldsymbol{\varphi}}_K + \sum_{L=1}^{n_{\text{tn}}} \mathbf{K}^{JL}_{\tilde{\Phi}\tilde{\Phi}} \, \mathrm{d}\tilde{\boldsymbol{\Phi}}_L \doteq \mathbf{0} \end{aligned} \tag{7}$$

which defines the following iterations matrices:

$$\begin{aligned} \mathbf{K}^{IK}_{\bar{\varphi}\bar{\varphi}} &= \frac{\mathrm{d}\mathbf{R}^I_{\bar{\varphi}}}{\mathrm{d}\bar{\boldsymbol{\varphi}}_K} = \mathop{\mathbf{A}}_{t=1}^{n_{\text{tr}}} \nabla_\xi N^i_{\bar{\varphi}} \frac{\mathrm{d}\Pi}{\mathrm{d}\bar{F}} A \; \mathbf{n} \otimes \mathbf{n} \; \nabla_\xi N^k_{\bar{\varphi}} + \nabla_\xi N^i_{\bar{\varphi}} \Pi A \frac{1}{l} [\mathbf{I} - \mathbf{n} \otimes \mathbf{n}] \; \nabla_\xi N^k_{\bar{\varphi}} \\ \mathbf{K}^{IL}_{\bar{\varphi}\tilde{\Phi}} &= \frac{\mathrm{d}\mathbf{R}^I_{\bar{\varphi}}}{\mathrm{d}\tilde{\boldsymbol{\Phi}}_L} = \mathop{\mathbf{A}}_{t=1}^{n_{\text{tr}}} \nabla_\xi N^i_{\bar{\varphi}} \frac{\mathrm{d}\Pi}{\mathrm{d}\tilde{f}} \; A \; \mathbf{n} \otimes \mathbf{N} \; \nabla_\xi N^l_{\tilde{\Phi}} \\ \mathbf{K}^{JK}_{\tilde{\Phi}\bar{\varphi}} &= \frac{\mathrm{d}\mathbf{R}^J_{\tilde{\Phi}}}{\mathrm{d}\bar{\boldsymbol{\varphi}}_K} = \mathop{\mathbf{A}}_{t=1}^{n_{\text{tr}}} \nabla_\xi N^j_{\tilde{\Phi}} \frac{\mathrm{d}\pi}{\mathrm{d}\bar{F}} \; A \; \mathbf{N} \otimes \mathbf{n} \; \nabla_\xi N^k_{\bar{\varphi}} \\ \mathbf{K}^{JL}_{\tilde{\Phi}\tilde{\Phi}} &= \frac{\mathrm{d}\mathbf{R}^J_{\tilde{\Phi}}}{\mathrm{d}\tilde{\boldsymbol{\Phi}}_L} = \mathop{\mathbf{A}}_{t=1}^{n_{\text{tr}}} \nabla_\xi N^j_{\tilde{\Phi}} \frac{\mathrm{d}\pi}{\mathrm{d}\tilde{f}} \; A \; \mathbf{N} \otimes \mathbf{N} \; \nabla_\xi N^l_{\tilde{\Phi}} + \nabla_\xi N^j_{\tilde{\Phi}} \; \pi A \frac{1}{L} \; [\mathbf{I} - \mathbf{N} \otimes \mathbf{N}] \; \nabla_\xi N^l_{\tilde{\Phi}} \end{aligned} \tag{8}$$

Note that the first term of each right-hand side is associated with the material stiffness matrix while the second term is typically referred to as the geometric stiffness matrix in structural mechanics. For the Neo-Hookean case, the linearizations of the stresses Π and π that enter the material stiffness contribution read

$$\frac{\mathrm{d}\Pi}{\mathrm{d}\bar{F}} = \frac{1}{2} E_0 \left[\frac{1}{\tilde{f}} + \frac{\tilde{f}}{\bar{F}^2} \right] \quad \frac{\mathrm{d}\Pi}{\mathrm{d}\tilde{f}} = -\frac{1}{2} E_0 \left[\frac{1}{\bar{F}} + \frac{\bar{F}}{\tilde{f}^2} \right] = \frac{\mathrm{d}\pi}{\mathrm{d}\bar{F}} \quad \frac{\mathrm{d}\pi}{\mathrm{d}\tilde{f}} = \frac{1}{2} E_0 \left[\frac{\bar{F}^2}{\tilde{f}^3} + \frac{1}{\tilde{f}} \right] \tag{9}$$

Copyright © 2005 John Wiley & Sons, Ltd.

while the linearizations of spatial and material normals $\mathbf{n}$ and $\mathbf{N}$ that basically define the geometric stiffness contribution take the following representation:

$$\frac{\mathrm{d}\mathbf{n}}{\mathrm{d}\bar{\boldsymbol{\varphi}}_k} = \frac{1}{l}[\mathbf{I} - \mathbf{n} \otimes \mathbf{n}]\nabla_\xi N_k, \quad \frac{\mathrm{d}\mathbf{n}}{\mathrm{d}\tilde{\boldsymbol{\Phi}}_l} = \mathbf{0} = \frac{\mathrm{d}\mathbf{N}}{\mathrm{d}\bar{\boldsymbol{\varphi}}_k}, \quad \frac{\mathrm{d}\mathbf{N}}{\mathrm{d}\tilde{\boldsymbol{\Phi}}_l} = \frac{1}{L}[\mathbf{I} - \mathbf{N} \otimes \mathbf{N}]\nabla_\xi N_l \tag{10}$$

The solution of the coupled system of Equations (7) finally defines the iterative update for the spatial and material joint point positions $\bar{\boldsymbol{\varphi}}_K = \bar{\boldsymbol{\varphi}}_K + \mathrm{d}\bar{\boldsymbol{\varphi}}_K$ and $\tilde{\boldsymbol{\Phi}}_L = \tilde{\boldsymbol{\Phi}}_L + \mathrm{d}\tilde{\boldsymbol{\Phi}}_L$. Recall that the set of equations (7) defines a monolithic solution technique. A staggered solution scheme follows straightforwardly by setting $\mathbf{K}^{IL}_{\bar{\varphi}\tilde{\Phi}} = \mathbf{0}$ and $\mathbf{K}^{JK}_{\tilde{\Phi}\bar{\varphi}} = \mathbf{0}$, see Reference [13].

3. RESULTS

This section treats two different trusses, a simple truss which is used as a benchmark problem in order to have a quality measure for the introduced procedure and a more sophisticated bridge structure. In all of the examples, the following data is used, $E_0 = 10000$, $A = 1$, $L = 100$.

3.1. *Example I—Benchmark problem*

First, we study a simple truss structure consisting of 8 nodes and 13 members. For the spatial motion problem only the leftmost and rightmost nodes are constrained, whereas for the material motion problem only the three topmost nodes are allowed to move in the vertical direction, cf. Figure 2, left. Due to a symmetric load case and symmetric member connectivity, a symmetric solution is expected. This justifies the constraint $L_6 = L_{10}$, with L_6 and L_{10} being the length of the members 6 and 10, respectively. An analytical solution can be constructed by assuming infinitesimal strains. Since the truss is statically determinate, all member forces $S_i = S_i(P, L_6, L_8)$ can be computed as a function of the given external load P and the unknown

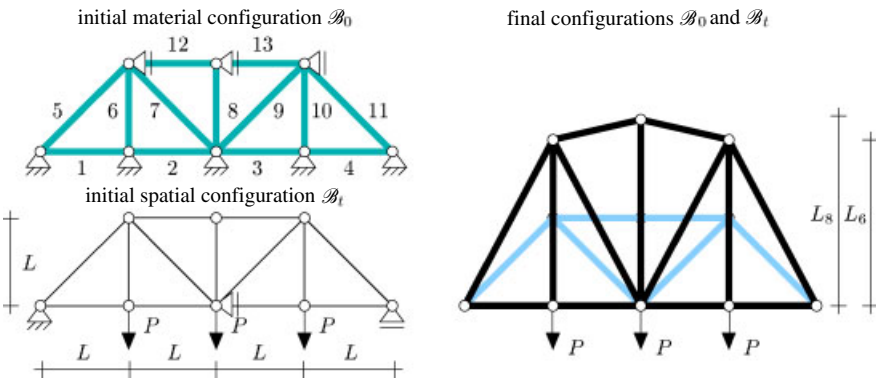

Figure 2. Benchmark problem—material and spatial configuration, initial state (left) and final state (right).

Copyright © 2005 John Wiley & Sons, Ltd.

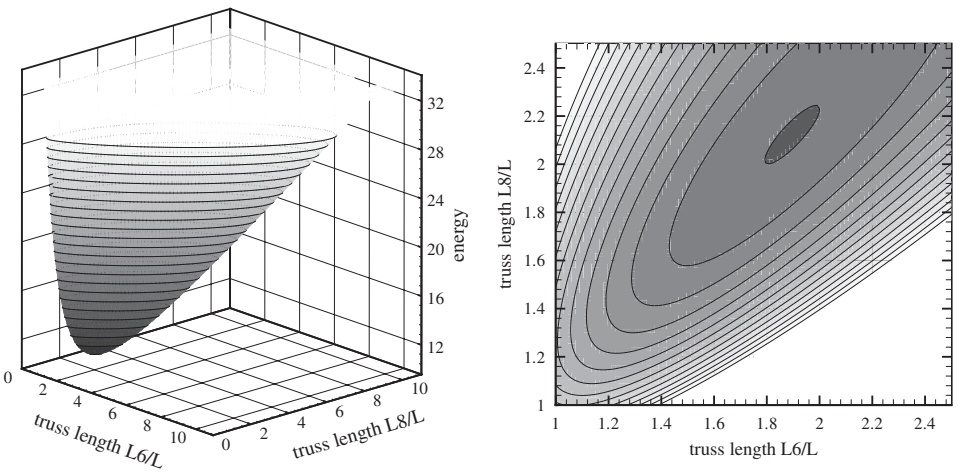

Figure 3. Benchmark problem—complementary energy vs truss lengths L_6/L and L_8/L.

geometry L_6 and L_8. The complementary energy $\mathscr{I}^c$ can then be elaborated as follows:

$$\mathscr{I}^c(P,L_6,L_8)=\frac{L}{2EA}\left[S_1^2+S_2^2+S_3^2+S_4^2+[S_5^2+S_7^2+S_9^2+S_{11}^2]\sqrt{1+L_6^2/L^2}\right.$$
$$\left.+[S_6^2+S_{10}^2]L_6/L+S_8^2L_8/L+[S_{12}^2+S_{13}^2]\sqrt{1+[L_8-L_6]^2/L^2}\right]$$

The minimization of the complementary energy with respect to unknown geometry L_6 and L_8 defines the analytical solution of the linear problem as $L_6\approx 1.88L$ and $L_8\approx 2.11L$. Figure 3 illustrates the complementary energy $\mathscr{I}^c$ as a function of the member truss lengths L_6 and L_8 which obviously takes a minimum at the analytical solution of $L_6\approx 1.88L$ and $L_8\approx 2.11L$.

Next, we analyse the truss of the benchmark problem numerically with an external load of $P=1$, thus using the non-linear algorithm suggested in Section 2 but being in the linear range due to the small amount of loading. We start with a symmetric initial configuration with $L_6=L_8=L_{10}=L$ as illustrated in Figure 2. The monolithic Newton–Raphson scheme converges quadratically within six iterations, cf. Table I. The numerical solution of $L_6\approx 1.88L$ and $L_8\approx 2.11L$ illustrated in Figure 2, right, agrees perfectly with the analytical solution. Figure 2, right, nicely documents that due to the restriction to the geometrically linear case, the final material and the final spatial configuration are nearly identical. When increasing the load to enter the non-linear regime, e.g. to $P=100$, we find increased member lengths of $L_6\approx 1.91L$ and $L_8\approx 2.13L$, whereby the optimal solution is again found within six iterations. Even a non-symmetric initial configuration with, e.g. $L_6=0.6L$, $L_8=1.3L$ and $L_{10}=1.1L$ leads to the same symmetric solution, however, now, within eight iterations. Figure 4 illustrates the evolution of the material and spatial configurations $\mathscr{B}_0$ and $\mathscr{B}_t$ at different stages of the iteration. In the geometrically linear limit analysed herein, both configurations are, of course,

Copyright © 2005 John Wiley & Sons, Ltd.

Table I. Benchmark problem—quadratic convergence of Newton iteration.

Iteration	Residual
Iteration 0	1.42853−03
Iteration 1	5.3876e−01
Iteration 2	3.6251e−01
Iteration 3	5.3244e−02
Iteration 4	2.8629e−04
Iteration 5	6.9799e−08
Iteration 6	5.9242e−12

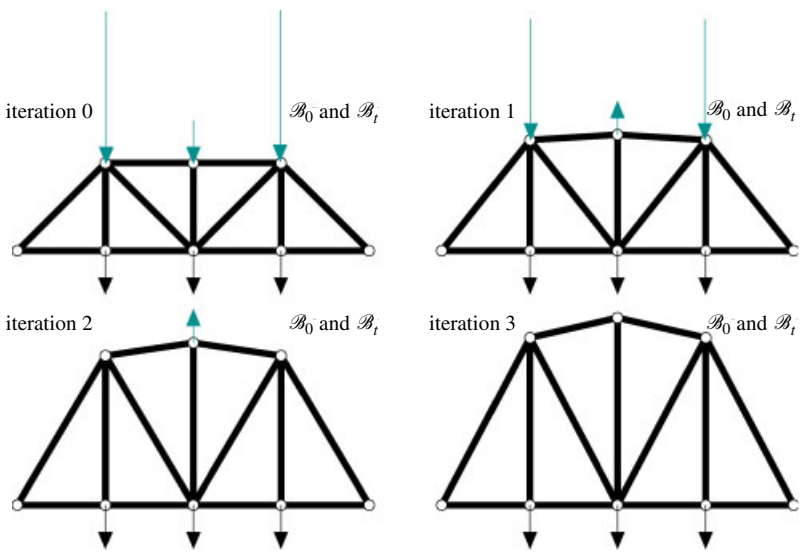

Figure 4. Benchmark problem—evolution of material and spatial configurations and forces during the iteration.

nearly identical and the difference between $\mathscr{B}_0$ and $\mathscr{B}_t$ is hardly visible. The series of Figure 4 nicely demonstrates the successive reduction of the material forces on the top nodes during the iteration.

3.2. *Example II—Bridge structure*

Secondly, we consider the truss shown in Figure 5, left. The leftmost and the rightmost nodes are fixed in the spatial motion problem. For the material motion problem all lower nodes are fixed and the upper nodes are allowed to move vertically. Under the influence of the applied load of $P = 100$, a material force residual develops for any material degree of freedom, cf. Figure 6. The coupled system of Equations (7) aims at letting the spatial and material force residuals vanish at all unconstrained degrees of freedom. Energy is released as nodes move opposite to the material force residual. Figure 6 shows the evolution of the solution during the

Copyright © 2005 John Wiley & Sons, Ltd.

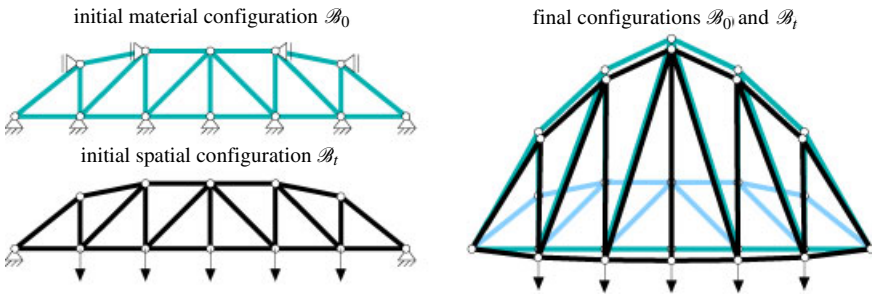

Figure 5. Bridge structure—material and spatial configuration, initial state (left) and final state (right).

Table II. Bridge structure—quadratic convergence of Newton iteration.

Iteration	Residual
Iteration 0	1.0117e+02
Iteration 1	4.6107e+02
Iteration 2	4.6107e+02
Iteration 3	2.0262e+02
Iteration 4	9.4013e+01
Iteration 5	5.8295e+01
Iteration 6	5.4107e+00
Iteration 7	3.8514e−02
Iteration 8	1.4768e−05
Iteration 9	1.0128e−11

iterations. In the optimized configuration, which is found after eight iterations, all residuals vanish. This is inherent to optimizing the potential energy with respect to the material joint positions. The optimal vertical positions of the top nodes resemble a parabola, cf. Figure 5, right. The evolution of the maximum deflection of the floor joints from $0.629L$ to $0.176L$ for the optimal structure clearly reveals that the structure becomes stiffer due to the optimization procedure. During the iteration, the algorithm converges quadratically towards the optimal solution as indicated through the evolution of the residuals in Table II. Nevertheless, quadratic convergence can only be found close to the solution. Within the first three iterates, the iterative solution is far away from the optimal bridge structure, which is underlined nicely by the plots of the corresponding configurations $\mathscr{B}_0$ and $\mathscr{B}_t$ in Figure 6. After the first four iterations, however, the algorithm converges quadratically and configurational changes are only of minor order.

We observed that the optimized configuration is independent of the starting configuration. Of course, the optimal configuration depends on the loading conditions and on the material parameters which means that other initial conditions will in general lead to other optimal positions of the nodes. Note that in contrast to the spatial motion problem alone, the coupled spatial and material motion problem might generally be non-convex. Due to the high degree of non-linearity one can thus in general not state whether the solution found is a local or a global optimum.

Copyright © 2005 John Wiley & Sons, Ltd.

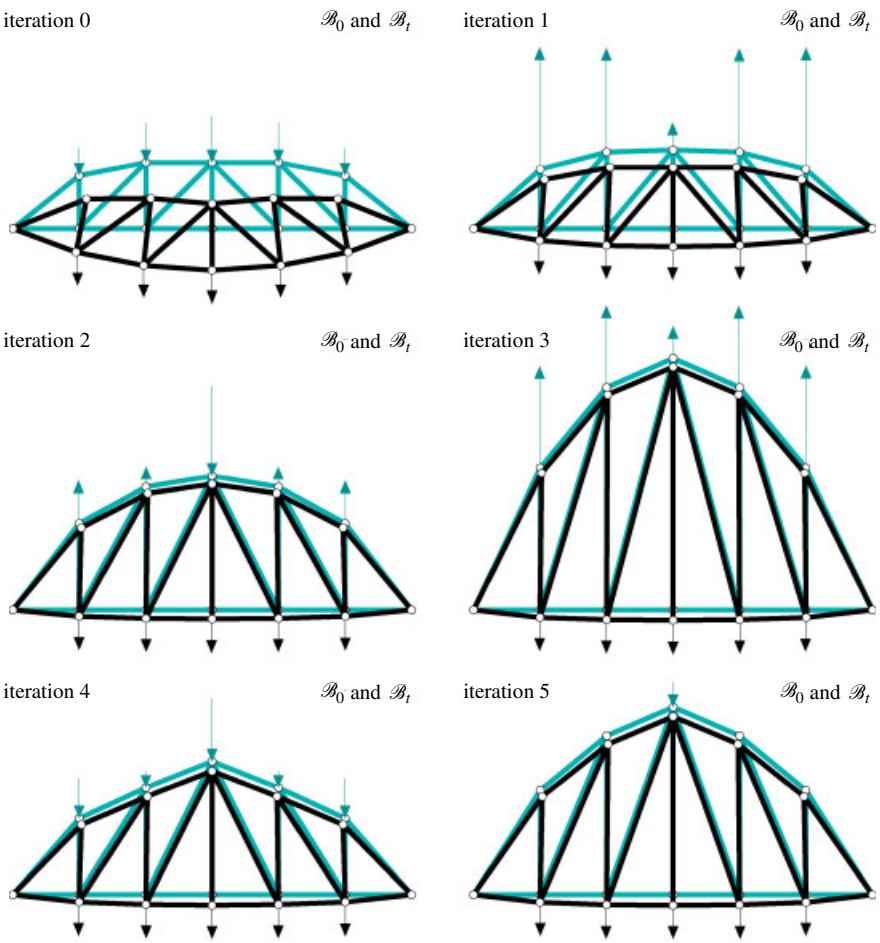

Figure 6. Bridge structure—evolution of material and spatial configurations and forces during the iteration.

4. CLOSURE

A dual equilibrium formulation is used for the shape optimization of truss geometries. Both the co-ordinates of the joints in the spatial (deformed) domain and in the material (undeformed) domain are taken as unknowns. The conjugated variables are denoted as the spatial forces and the material forces, respectively. The dual equilibrium problem consists of the simultaneous equilibration of spatial forces and material forces. The general discrete dual equilibrium problem for trusses has been presented, whereby each joint has two degrees of freedom (one spatial, one material) for every spatial dimension. Consistent linearization results in a fully coupled system of equations, which is solved with an incremental iterative Newton–Raphson scheme.

Copyright © 2005 John Wiley & Sons, Ltd.

Two examples have been studied. The first example concerns a benchmark test with a known analytical solution for the case of infinitesimal strains. It is shown that different initial configurations lead to the same optimized configuration, which provides evidence for the robustness of the proposed method. In the second example the evolution of the material force residuals is tracked, and it is shown that vanishing material force residuals correspond to optimal material co-ordinates of the joints.

The minimization of the potential energy with respect to the material co-ordinates provides a promising approach towards the shape optimization of truss structures. Unlike the classical spatial motion problem, however, the coupled spatial and material motion problem is generally non-convex. Accordingly, it cannot be ensured that the optimal solution found by the proposed algorithm corresponds to the global optimum. The analysis of alternative solution schemes is part of a current research project.

ACKNOWLEDGEMENTS

The authors would like to thank Professor Manfred Braun from the University of Duisburg-Essen, Germany, for fruitful discussions on the presented approach.

REFERENCES

1. Haftka RT, Gürdal Z. *Elements of Structural Optimization* (3rd edn). Kluwer: Dordrecht, 1992.
2. Braun M. Configurational forces induced by finite-element discretization. *Proceedings of Estonian Academic Sciences of Phys. Math.* 1997; **46**:24–31.
3. Braun M. Structural optimization by material forces. In *Mechanics of Material Forces—EuroMech Colloquium 445*, Steinmann P, Maugin GA (eds), Kaiserslautern, 2003; 211–218.
4. Eshelby JD. The force on an elastic singularity. *Philosophical Transactions of the Royal Society of London* 1951; **244**:87–112.
5. Eshelby JD. The elastic energy–momentum tensor. *Journal of Elasticity* 1975; **5**:321–335.
6. Maugin GA. *Material Inhomogeneities in Elasticity*. Chapman & Hall: London, 1993.
7. Kienzler R, Herrmann G. *Mechanics in Material Space with Applications to Defect and Fracture Mechanics*. Springer: Berlin, Heidelberg, New York, 2000.
8. Steinmann P. On spatial and material settings of hyperelastodynamics. *Acta Mechanica* 2002; **156**:193–218.
9. Steinmann P. On spatial and material settings of thermo-hyperelastodynamics. *Journal of Elasticity* 2002; **66**: 109–157.
10. Mueller R, Maugin GA. On material forces and finite element discretizations. *Computational Mechanics* 2002; **29**:52–60.
11. Thoutireddy P, Ortiz M. A variational *r*-adaption and shape optimization method for finite-deformation elasticity. *International Journal for Numerical Methods in Engineering* 2004; **61**:1–21.
12. Kuhl E, Askes H, Steinmann P. An ALE formulation based on spatial and material settings of continuum mechanics. Part 1: Generic hyperelastic formulation. *Computer Methods in Applied Mechanics and Engineering* 2004; **193**:4207–4222.
13. Askes H, Kuhl E, Steinmann P. An ALE formulation based on spatial and material settings of continuum mechanics. Part 2: Classification and applications. *Computer Methods in Applied Mechanics and Engineering* 2004; **193**:4223–4245.

Copyright © 2005 John Wiley & Sons, Ltd.